Department of AERONAUTICS and ASTRONAUTICS
STANFORD UNIVERSITY

temp 6835

Second Semiannual Progress Report

ADDITIONAL STUDY AND FURTHER DEVELOPMENT OF THE TRACER-SPARK TECHNIQUE FOR FLOW-VELOCITY MEASUREMENTS

Contract No. NsG-620

Subject:

An Experimental Study of the
Width and Temperature of Sparks
used for Flow-Velocity Measurements

by
James B. Kyser

Submitted to the
National Aeronautics and Space Administration
by the
Department of Aeronautics and Astronautics

Stanford University
Stanford, California

May 1965

Second Semiannual Progress Report

ADDITIONAL STUDY AND FURTHER DEVELOPMENT OF THE TRACER-SPARK TECHNIQUE FOR FLOW-VELOCITY MEASUREMENTS

Contract No. NsG-620

Subject:

An Experimental Study of the
Width and Temperature of Sparks
used for Flow-Velocity Measurements

by
James B. Kyser

Submitted to the
National Aeronautics and Space Administration
by the
Department of Aeronautics and Astronautics

Stanford University

Stanford, California

May 1965

I. INTRODUCTION

For the past year, the Department of Aeronautics and Astronautics at Stanford University has been studying methods of improving the resolution of tracer-spark measurements of flow velocity. The principle of operation and the development of electrodes incorporating a magnetic field for confining the spark, together with velocity measurements made with these electrodes, were discussed in the first semiannual progress report (Reference 1). During the past six months work has been concentrated on photographic studies of spark width and spectrographic studies of spark temperature.

The purposes of the photographic study of spark width were:

1) To investigate the effect of spark strength, static pressure and magnetic field strength on the photographed spark width.

2) To deduce the distribution of ionization in the initial spark column so that the diffusion of the ionized column can be analyzed and the effect of this diffusion on later sparks thus determined.

The spectrographic study of spark-column temperature was undertaken to ascertain the extent of the spark heating of the gas and to investigate the effects of spark strength, static pressure, and magnetic field strength on such heating.

Nominal test conditions in the Stanford spark-heated wind tunnel in which the tracer-spark technique has been used to measure flow velocity (Reference 1) are: static pressure = 1 mm Hg, spark strength = 0.5 joules, magnetic field strength = 500 gauss. In these studies, pressure was varied from 0.1 mm to 10 mm, spark strength was varied from 0.05 joules to 5.0 joules and magnetic field strength was varied from 0 to 655 gauss. A wider range of field strengths was considered desirable, but was not attempted because of the complexity.

The details of the two studies, including the results, are discussed in the following sections.

II. PHOTOGRAPHIC STUDIES OF SPARK WIDTH

Experimental Procedure

The studies of spark width were conducted in the static test chamber shown in Figure 1. Sparks were struck between electrode tips spaced five inches apart. Two magnetic coils were carefully positioned so that the common axis of the coils contained the two electrode tips, making the magnetic field lines parallel to the spark-column axis.

The test gas was kept pure by continuous flushing with bottled nitrogen. Test-chamber pressure was read on an Alphatron gauge and was kept at the desired level by throttling the vacuum pump or varying the flow rate from the nitrogen bottle. Sufficient pumping capacity was available to insure a change of gas in the test chamber every two seconds. The magnetic coil was energized and the spark was fired every 12 seconds by a Teletronix 160-series waveform and pulse generator. Thus, the gas in the static chamber was changed at least six times between successive sparks.

One end of the static test chamber was made for mounting a Fairchild type-F-296 oscilloscope camera for photographing the spark. Since the camera had no provision for focusing, the mount was constructed so that the plane of the spark was permanently in focus. The camera-mount dimensions were critical because at an aperture setting of f/1.9, the lens on the camera had a depth of field of only one-quarter inch. The arrangement worked quite well, however, because of the large (0.9 actual size) image and the accurate placement of the image at the center of the film. It was necessary to leave the camera shutter open for several seconds, as there was no synchronization between shutter and spark, but no problems were encountered with excessive exposure from background lighting. Polaroid type-46L film was used for photographing the sparks because a transparency was needed for analysis of the photographs. Although some difficulty with non-uniformity was experienced, the ease of developing the film more than made up for the tests that had to be repeated as a result of the non-uniformity.

The spark photographs were analyzed by using an optical comparator and a photomultiplier tube as a densitometer. The comparator had a magnification factor of 62.5, and the photomultiplier entrance slit was 1/16 inch wide. Consequently, the resolution of the system was 0.001 inches on the photograph scale. The position could be read to an accuracy of 0.001 inches by means of a dial-indicator gauge. Since densitometers are widely available commercially, further details will not be given.

Discussion of Results

The spark-width data obtained in the study are given in Figure 2, and are plotted as relative intensity versus spark width. The parameters were varied over the ranges indicated below:

Spark strength:
- a) 5.0 joules (0.1 μf, 10 KV)
- b) 0.5 joules (0.01 μf, 10 KV)
- c) 0.1 joules (0.001 μf, 15 KV)

Static Pressure:
- a) 0.1 mm (for 0.5 joule spark only)
- b) 0.5 mm
- c) 2.0 mm
- d) 10.0 mm (for 0.5 joule spark only)

Magnetic Field:
- a) 0 gauss
- b) 225 gauss
- c) 445 gauss
- d) 655 gauss

Damping resistors were used to provide 64% of critical damping in all test conditions except for those with 10-mm static pressure. At 10-mm static pressure the spark gap itself appeared to have resistance sufficient to prevent the discharge from oscillating.

In Figure 2 the intensity profiles are seen to have a shape generally like a gaussian distribution. The profiles are not given outside the 10-percent to 90-percent relative-intensity range because the film non-uniformity made the data erratic at each end of the scale. The problem of film non-uniformity was made more severe by the low exposure levels required to prevent a distortion of the spark profile from over-exposure

at the center of the spark.

The most significant thing shown by the intensity profiles in Figure 2 is the narrow spark width at the 90% intensity level. At this level, the widest spark without magnetic field was 0.25 inches, and the widest spark with a 655-gauss magnetic field was 0.08 inches. If a densitometer is to be used for the analysis of a spark photograph, it can be assumed that the effective width of the spark will be the width at 90% intensity, and that the spark center can be located to an accuracy of about 10% of this effective width. Thus, the "reading" error would be a maximum of 0.025 inches for the tests with no magnetic field and 0.008 inches for the tests with a 655-gauss magnetic field. If the spark-location measurements were part of a flow-velocity measurement involving two such sparks separated by a distance of about 5 inches, the maximum expected reading error for the tests without a magnetic field would be about 1% of this distance for each spark or about 2% total. For the tests with a 655-gauss field, the maximum total reading error would be 2/3%. Thus, on the basis of reading error alone, the use of a magnetic field to reduce spark width might not be justified if data are to be analyzed with a densitometer.

If data are to be analyzed using the un-aided eye to locate the center of the spark on the photographs, it can be assumed that the effective spark width would be the width at 50% relative intensity. In Figure 3 the spark width at this intensity is plotted versus magnetic field strength. In Figure 3(b) a three-fold reduction in spark width can be seen in the 0.1-mm-pressure tests as magnetic field strength is increased from zero to 225 gauss; whereas in the 10-mm-pressure tests, an increase in field strength from zero to 655 gauss caused a reduction in spark width of only one-third. Also, a comparison of the 0.5-mm and 2.0-mm-pressure data in Figures 3(a), 3(b), and 3(c) shows that increasing magnetic field causes the greatest reduction in spark width with the 0.001 μf capicitor and the smallest reduction in spark width with the 0.1 μf capacitor. Thus, the magnetic field is most effective in reducing the spark width in tests at low pressures or with small capacitors.

The maximum effective spark width to the un-aided eye was 1.1

inches in the tests with no magnetic field and 0.37 inches in the tests with a 655-gauss field. If the reading error is again assumed to be 10% of the apparent spark width, the maximum reading error would be 0.11 inches for the tests with no magnetic field and 0.037 inches for the tests with a 655-gauss field. If the readings were a part of the velocity measurement discussed previously, a maximum total reading error of 4 1/2% would be expected for the cases with no magnetic field. A corresponding value of 1 1/2% would be expected with a 655-gauss field. Thus, for the conditions of these static tests, a densitometer appears as effective as a magnetic field in reducing the reading error due to spark width. At lower densities the magnetic field would be expected to be more effective; at higher densities the densitometer would be more effective.

Although a diffuse spark appears to be of no great disadvantage in the analysis of data, it might offer a poorly defined path for the second spark, and thus be detrimental to be measuring accuracy. The effect of the magnetic field in concentrating the light from the spark can be seen in Figure 4. The data shown in Figure 4 are the same data shown in Figures 2(d) and 2(e) but adjusted so that there is an equal area under each curve. The justification for this is the experimental observation that the total light output, as measured by a photomultiplier tube, is unaffected by magnetic field strength. Since the spark light is produced primarily by electron-molecule collisions, it may be assumed that the electron density and the ionization level are also proportional to the light-intensity curves. The effect of the magnetic field, on the basis of these assumptions, is to concentrate the ionization in a small area with well-defined boundaries in the center of the spark column. If we neglect diffusion effects, the second spark, as a result of this concentration, will be more apt to strike through the center of the original spark column. Also, it will be more apt to be narrow with well-defined boundaries, as has been observed experimentally.

It should be noted that Figure 4 does not represent the radial distribution of intensity, electrons, or ionization level. Instead, it is a one-dimensional representation of a two-dimensional object,

and so each point represents an integration of intensity over a range of radii. Further work is required to reduce the data presented in Figures 2 and 4 to radial distribution of intensity or ionization level. Once this is done, the spark-column-diffusion problem can be studied analytically, with this data on the radial distribution of ionization level as initial conditions for the diffusion process. As discussed in Reference 1, diffusion of the spark column is expected to be one of the factors limiting the applicability of the tracer-spark technique.

III. SPECTROGRAPHIC STUDIES OF SPARK TEMPERATURE

Exploratory Study of Spark Spectrum

As a first step in the spectrographic studies of spark temperature, several spectrographic plates were made of the spark spectrum. From these plates it could be seen that the dominant contribution to the spark radiation is the nitrogen second-positive band system. Several bands from the nitrogen first-negative system were seen, but these were weak compared with the strongest bands in the second-positive system. No trace was found of the first-positive system.

The time-resolved intensity of the second-positive system was measured with a Dumont 6292 photomultiplier tube and a colored-glass filter that passed wavelengths between 3400 and 4400 Angstroms. In a similar manner, the time-resolved intensity of radiation at longer wavelengths was measured with a Dumont 6911 photomultiplier tube and a colored-glass filter that passed wavelengths above 6500 Angstroms. It is presumed that the first-positive band system was the dominant contributor to the radiation at these wavelengths.

The foregoing measurements showed that the short-wavelength (or violet) radiation varied with time in the same manner as the current, but that the long-wavelength (or red) radiation reached a maximum about the time the current ceased and then decayed exponentially. This behavior can be predicted from data on upper-state lifetimes given in Reference 2. The lifetime of the upper state in the second-positive system is about 0.05 μs , while the lifetime of the upper state in the first-positive

system is about 5 μs. Therefore, on a microsecond time scale, the second-positive system would appear to respond instantly to changes in excitation rate, while the first-positive system would appear to lag badly. This lag in radiation could cause blurring of photographs of sparks in a moving stream. Since the first-positive system includes radiation at wavelengths as short as 4723 A, it is probably advisable to remove this system by filtering even though its intensity is low.

As a final step in the exploratory study of the spark spectrum, the effects of changes in density and magnetic field on the violet and red radiation were measured. It was observed that the magnetic field had no detectable effect on the peak intensity or the time variation of either the red or the violet radiation. An increase in density caused the red radiation to increase in intensity more than the violet. Since the second-positive system has a higher excitation energy than the first-positive system, the implication is that the electron temperature decreases as a result of an increase of density.

Experimental Procedure for Temperature Measurements

The spectrographic studies of spark temperature were conducted with the static test chamber shown in Figure 1, and the test procedures followed in the previous section were followed here also. A collimating lens was attached to the camera adapter to increase the light available for spectrographic analysis. The instrumentation used to make the spark-temperature measurements is shown in Figure 5.

A Jarrel Ash half-meter spectrometer was used to resolve the spark spectrum, and a Dumont 6292 photomultiplier tube was used to measure the time variation in intensity of the selected part of the spectrum. The spectrometer setting was changed between sparks, permitting a time-resolved spectrum to be obtained. Since data at each different wavelength were obtained from a different spark, a second Dumont 6292 photomultiplier tube was used to monitor the light from the spark to insure that all sparks were of equal intensity. All data were recorded on a Tektronix 551 oscilloscope.

Attempts have been made to measure spark temperature using each of the three band systems identified in the spark spectrum. Since the second-positive system is the most prominent of the three, most of the effort has been directed towards analysis of this system.

Computed Band Structure

The second-positive band system in the nitrogen spectrum is composed of a series of regularly spaced bands with most of the energy in the 3000 A to 4500 A range. The bands have a sharp "head" on the long-wavelength side, and their intensity gradually fades out on the short-wavelength side. Vibrational temperatures can be found by examining the intensity distribution from band-to-band; rotation temperature can be found by examining the intesity distribution within the bands. Before temperature measurements can be made, however, it is necessary to compute intensity distributions over the anticipated temperature range to establish the relation between intensity distribution and temperature.

The intensity distribution within the bands was computed with the aid of equations and constants found in Reference 3. Except for the point discussed in the next paragraph, the procedure was straightforward, so it need not be discussed in great detail in this report.

The structure within a single band in the nitrogen spectrum is composed of a large number of lines. Each line corresponds to a single rotational transition, and the lines can be grouped into families or "branches", depending on whether the change in rotational quantum number is -1, 0, or +1. Because the molecular states in the transition responsible for the second-positive system are triplet states, the branches are split into three sub-branches. Each sub-branch has lines spaced at intervals of one Angstrom or less. As a result, the band structure will appear to be a continuum distribution unless the examing instrument has a resolution better than about 0.1 Anstrom. Since the instrument used had a resolution of about 0.3 Anstrom, it appeared advisable to compute the intensity distribution as if it were a continuum distribution. A slight simplification was achieved by ignoring triplet splitting and considerating all sub-branches lumped into their respective branches.

The computed intensity distribution within the 0,2 band is shown in Figure 6 for several equilibrium rotational temperatures. The 0,2 band was selected because is represented the most favorable combination of intensity and photomultiplier sensitivity. The computed continuum distribution has been integrated across the measured instrument-response profile to give the normalized intensity distribution shown in Figure 6. The band head actually occurs at 3805 A, but the region near the band head is characterized by large changes in intensity with changing wavelength, so it has not been used for temperature measurement. The intensity data shown in Figure 6 have been normalized with respect to the integrated intensity at 3795 A. From this figure, it can be seen that rotational temperature can be expressed as a unique function of the ratio of intensities at any two wavelengths. For the range of rotational temperatures between $300^{\circ}K$ and $500^{\circ}K$, the ratio of the intensity at 3785 A to that at 3795 A offers good sensitivity to temperature, and was therefore used for data analysis in these studies. In Figure 7, this intensity ratio has been plotted as a function of temperature for three different measured instrument-response profiles. The three profiles correspond to slit-widths of 100μ, 200μ, and 400μ, and have pass bands of 1.7A, 3.4A and 6.8A respectively.

Experimental Results

Preliminary spectrometer data showed the gas in the spark column to have an equilibrium intensity distribution superimposed upon a small amount of continuum radiation. Since the intensity distribution corresponded to an equilibrium rotational temperature, it is assumed that the rotational temperature is representative of the temperature in the equation of state of the gas, and therefore rotational temperature will be referred to as temperature in the following discussions.

The intensity of the continuum was evaluated by measuring the intensity of radiation on either side of the band. Although the edge of the band is well defined only on one side (the head), the intensity at moderate equilibrium temperatures dies out sufficiently rapidly on the other side for the band to be thoughtof as having boundaries. The

intensity ratio on either side of the band was found to be about 0.05 on the scale in Figure 6, and was subtracted from the band intensity by using a continuum intensity trace as a "zero" trace for each measurement. Four sparks were therefore required for a single temperature measurement. The information obtained from each spark was:

a) Intensity at 3795 A
b) Intensity of continuum, read at 3815 A
c) Intensity at 3785 A
d) Intensity of continuum, read at 3815 A

Intensity ratio, as plotted in Figure 7, was then computed by dividing c) minus d) by a) minus b), and temperature was read from Figure 7.

Spark temperatures were measured for the range of parameters listed below:

Spark Strength
a) 5.0 joules (0.1 μf, 10 KV)
b) 0.5 joules (0.01 μf, 10 KV)
c) 0.05 joules (0.001 μf, 10 KV)

Static Pressure
a) 0.1 mm
b) 0.33 mm
c) 1.0 mm
d) 3.0 mm
e) 10 mm (5.0 joule and 0.5 joule sparks only)

Magnetic Field:
a) 0 gauss
b) 335 gauss
c) 655 gauss

The spark duration and peak current are as follows:

a) 5.0 joule spark : 2.5 μs, 700 amps
b) 0.5 joule spark : 0.8 μs, 210 amps
c) 0.05 joule spark : 0.25 μs, 70 amps

Time-resolved spark temperatures measured for the 5.0-joule spark are shown in Figure 8. Generally, the data show the temperature to increase with time. The tests with no magnetic field show a consistently

greater heating rate as pressure was increased, whereas tests with magnetic field do not show this trend. This difference is probably caused by the tendency for the spark-column size to decrease with increasing pressure in the tests without magnetic field, while remaining relatively constant with increasing pressure in the tests with magnetic field. Thus, in the tests without magnetic field, the primary effect of increasing pressure is to increase the current density in the spark column.

The erratic nature of the data points in Figure 8 is probably caused by small differences in the four sparks used to obtain each temperature measurement. When the 0.5-joule and 0.05-joule-spark data were plotted in the manner of Figure 8, no clearly defined increase of temperature with time was seen. Because of this, it appeared that mean spark temperatures would have more meaning than instantaneous temperatures. Mean temperatures were found from the ratio of the areas under the intensity-time traces, rather than from the ratio of the instantaneous intensities. Mean temperatures are tabulated in Table 1 for all tests performed in the study.

An examination of Table 1 reveals that, except for the case discussed just previously, no uniform variation in mean temperature with density is seen. Therefore, for each spark strength tested, the mean temperatures were averaged over all pressures for each field strength. The averages are listed on the last line of each part of Table 1. Except for the 0.05-joule-spark data with no magnetic field, the averages show an increasing mean spark temperature with increasing spark strength or field strength.

Interpretation of Results

A set of average heating values can be obtained by subtracting the ambient temperature ($295^{\circ}K$) from the average temperatures listed in Table 1. This set, which is listed in Table 2, does not seem realistic when it is noticed that the 5-joule spark, representing 100 times as much energy as the 0.05-joule spark, does only three times as much heating. This discrepancy cannot be attributed to spark size because,

as discussed earlier, capacitance did not effect spark size except in tests without magnetic field where increasing capacitance made the spark narrower.

A more consistent set of heating rates can be obtained if it is noted that the molecules emitting the radiation used to deduce temperatures represent a group of molecules that has undergone a specific type of collision with electrons. Since these excitational collisions might add some translational or rotational energy to the emitters, the temperature of the emitters in the spark column might not be the same as the temperature of the non-emitting molecules.

Further evidence that the excitational collision adds energy other than the excitation energy, comes from measurements of vibrational temperature. These measurements show the vibrational temperature to be considerably in excess of 5,000^{o}K for all conditions tested. Since vibrational excitation has an extremely long relaxation time compared with either the relaxation time of rotational excitation or the spark duration, it is possible that a considerable increase in emitter energy resulted from the excitation collision, and that most of the rotational energy, but little of the vibrational energy, was transferred to other molecules through collisions before emission took place.

For this discussion, however, it will be assumed only that some process during excitation increased the average emitter temperature above the gas temperature by a yet unspecified amount. An estimate of the average temperature increase, due to the excitational collision, can be obtained by observing that the average heating due to the 5-joule spark, is no greater than 200^{o}K. Therefore, if heating is roughly proportional to spark energy, the heating due to the 0.05-joule spark should be small enough to be unmeasureable with the present measuring accuracy. Therefore, temperature measurements obtained with the 0.05-joule spark should not show any general spark heating, but should show only the average temperature increase of the emitter due to the excitation process.

Since the average temperature listed for the 0.05-joule spark with zero magnetic field is out of harmony with other zero-field temperatures or other temperatures obtained with this spark, it appears reasonable

to use the average of the zero-field values for the 0.5-joule and 0.05-joule sparks for this discussion. With the aforementioned assumptions, it is implied that the average temperature increase of the emitters due to the excitation process is $45^{\circ}K$. If this $45^{\circ}K$ is subtracted from the values listed in Table 2, the adjusted temperature increase due to spark-column heating, listed in Table 3, is obtained.

At present it is not known whether the values listed in Table 2 or in Table 3, are the correct ones for computing the final spark-column temperature. In either case, a good approximation can be made by adding twice the appropriate entry to the ambient temperature. The values for the 5.0-joule spark thus obtained, do not show good agreement with the 2μs values plotted in Figure 8 because the plotted results were obtained from the ratios of two small intensities and hence are subject to question.

Use of Other Band Systems

A check of the temperature measurements discussed above was made by examing the 0,1 band in the first-negative system, and using the data of Reference 4 to convert intensity distribution into temperature. For the reasons listed below, the accuracy of these measurements was not as good as desired:

a) The intensity of this band was much lower than the intensity of the second-positive band used for temperature measurement.

b) The instrument profiles used in Reference 2 could not be reproduced exactly with the spectrometer slits.

c) The sensitivity of intensity ratio to temperature was poor in the range of interest.

In spite of these factors, however, the agreement of these measurements with the measurements discussed earlier was well within the accuracy of measurement.

An attempt to measure the total spark heating without encountering the difficulty discussed in the previous section, was made with the

2,0 band of the first-positive system. The emitter-heating problem is avoided here because the long life time of the upper state in the transition should allow the rotational temperature of the emitters to reach equilibrium with the other molecules before emission occurs. To be more specific, the upper-state lifetime is about 5μs, while the time between collisions ranges between 0.005μs for the highest pressure tested and 0.5μs for the lowest pressure tested. Thus, between 10 and 1000 collisions might be expected to occur between excitation and emission. The radiation from this transition persists for several microseconds after the spark is extinguished, and thus one would expect the final portion of the radiation to reflect the final gas temperature after all spark heading has been completed. Satisfactory measurements with this band system have not been possible to date because of the low light levels and the consequently greater effect of the continuum radiation.

By the same arguments, the measurements taken at 10-mm pressure and listed in Table 1 should reflect spark-column temperature rather than emitter temperature. The upper-state lifetime here was 0.05μs, so about 10 collisions could be expected to occur between excitation and emission. If any relaxation of the temperature increase due to excitation did occur, it was masked by data scatter or effects of unknown origin.

IV. FUTURE WORK

The spark-width studies are complete except for the required additional data analysis previously discussed. Further experimental work, including instrumentation development, is required in the study of spark temperature. The plans are discussed in the following paragraphs.

As mentioned previously, a total of four sparks is required to obtain a single temperature measurement. Two of these are used in the measurement of intensity distribution of the band, and two are used to measure the continuum intensity. A considerable loss in experimental accuracy results from a lack of exact reproducibility from spark to spark.

To remedy this, the two-channel photomultiplier head shown in Figure 9, is being developed. A knife edge is used to split the spectrum into two parts at the spectrometer exit slit. One part will go in a straight path to a photomultiplier tube; the other will strike the mirror built onto the knife-edge assembly and go to a second photomultiplier tube. In this manner, the intensity at two different wavelengths can be measured with a single spark. The continuum intensity measurement will require a second spark, but this is not a serious deficiency as the continuum intensity is small compared with the band intensity.

All parts for the two-channel photomultiplier head have been fabricated, but it has not yet been adjusted and calibrated. Once this is done it will be used to repeat the data shown in Table 1. It is anticipated that the increased measurement accuracy will allow time-resolved spark temperatures to be obtained. The new head will also make it possible to obtain temperature measurements in a hypersonic flow field, and as a result, future testing will involve a wide range of stream conditions.

V. CONCLUSIONS

The study of spark width shows that wide sparks can be resolved sufficiently well with a densitometer that the use of a magnetic field to reduce spark width might not be necessary from the standpoint of the measurement of spark location. It does appear, however, that a magnetic field may be required to concentrate the ionization so that the second spark will strike through the center of the ionized path. Work on this point is continuing.

The study of spark-column temperature shows that if moderate spark energies and magnetic field strengths are used, peak spark-column temperatures will be no higher than $70^{\circ}K$ to $180^{\circ}K$ above stream temperature. Further measurements might allow these limits to be revised downward to $10^{\circ}K$ to $70^{\circ}K$. It has also been shown that if a magnetic field is not used for reducing spark width, the spark heating is decreased.

The significance of these values will not be understood completely until the problem is studied further. It can be noted, however, that a 180°K increase in temperature due to spark heating would cause a significant distrubance in a 50°K stream whereas a 10°K increase would have very little effect in a 300°K stream.

REFERENCES

1. Kyser, James B. National Aeronautics and Space Administration. First Semiannual Progress Report Contract No. NsG-620. November 1964.

2. Nicholls, R. W. "Transition Probabilities of Aeronomically Important Speclia". Annales de Geophysique. Tome 20, No. 2, Avril-Juin 1964.

3. Hertberg, G. "Spectra of Diatomic Molecules. D. van Nostrand and Co., New York, 1950.

4. Muntz, E. P. and Able, S. J. "The Direct Measurement of Static Temperatures in Shock Tunnel Flows". Proceedings Third Hypervelocity Techniques Symposium, March 1964.

TABLE 1. MEAN SPARK TEMPERATURE (^{o}K)

a) 0.05-Joule Spark

Pressure, mm	Magnetic Field, Gauss		
	0	335	655
0 .10	340	345	355
0 .33	330	325	350
1.0	375	355	335
3.0	360	360	405
average	350	345	360

b) 0.5-Joule Spark

Pressure, mm	Magnetic Field, Gauss		
	0	335	655
0.10	315	395	430
0 .33	310	385	355
1.0	385	375	355
3.0	300	320	407
10	340	350	430
average	330	365	395

c) 5.0-Joule Spark

Pressure, mm	Magnetic Field, Gauss		
	0	335	655
0.10	380	465	450
0.33	420	455	515
1.0	430	470	480
3.0	440	480	510
10	480	485	485
average	430	470	495

TABLE 2. AVERAGE TEMPERATURE INCREASE DUE TO SPARK HEATING

Spark Energy, Joules	Magnetic Field, Gauss		
	0	335	655
0.05	55	50	65
0.5	35	70	90
5.0	135	170	200

TABLE 3. ADJUSTED TEMPERATURE INCREASE DUE TO SPARK HEATING

Spark Energy, Joules	Magnetic Field, Gauss		
	0	335	655
0.05	10	5	20
0.5	-*	25	35
5.0	90	130	155

*Value calculated from measurements was negative

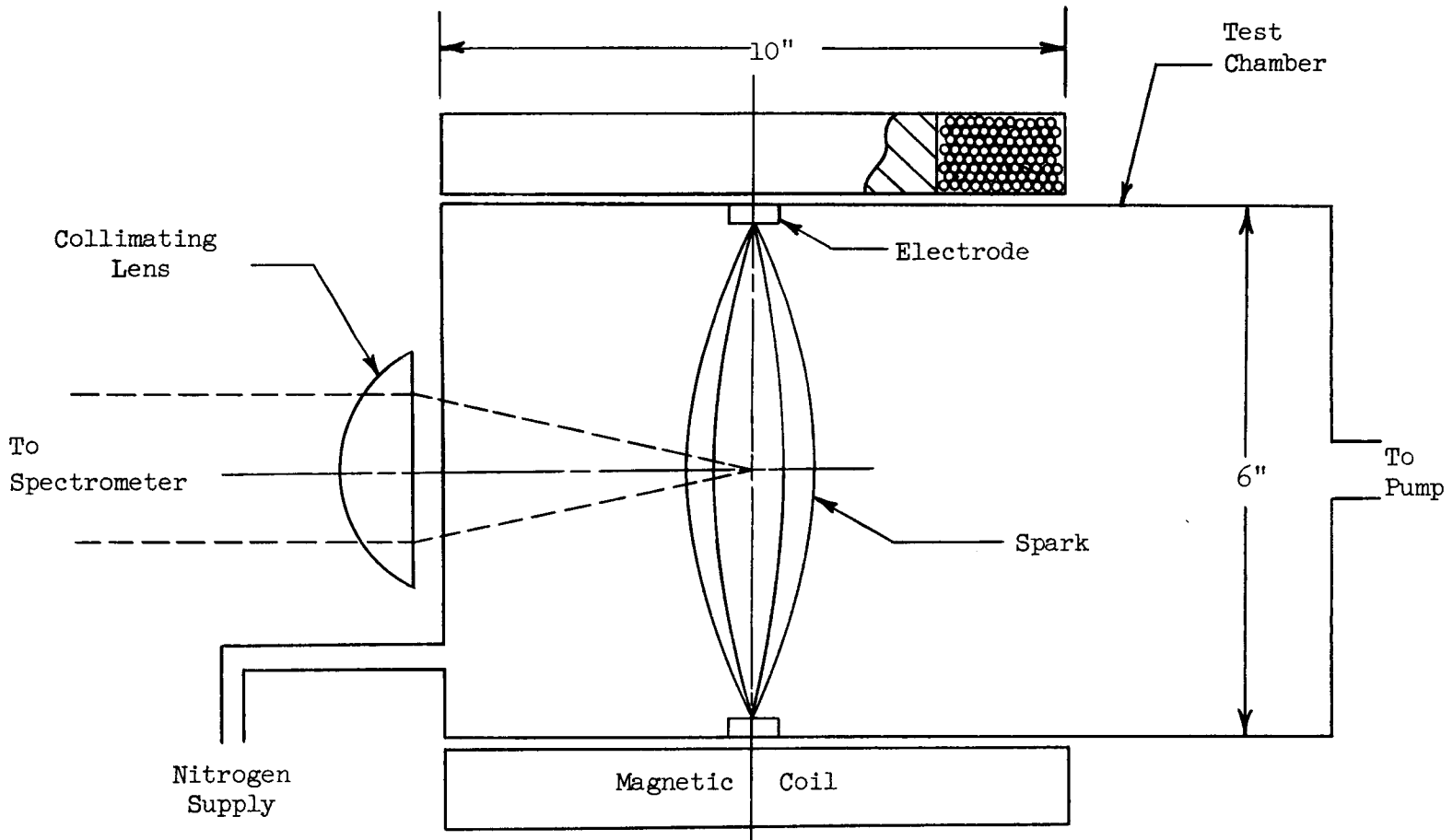

FIG. 1. STATIC TEST CHAMBER FOR SPARK-TEMPERATURE MEASUREMENT

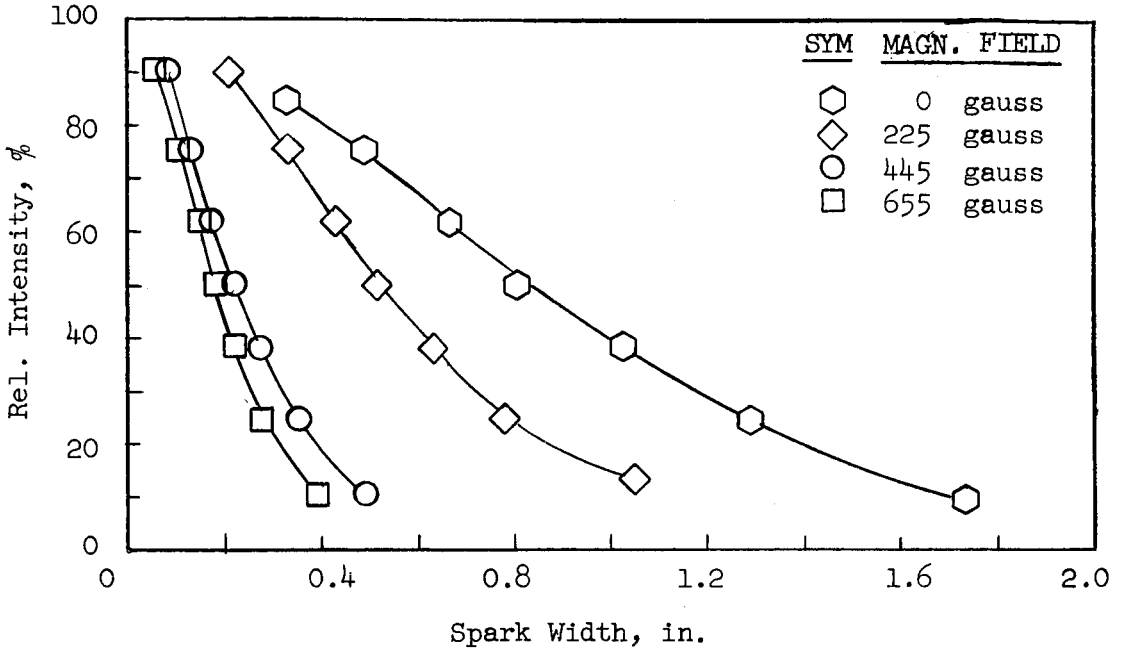

(a) 0.001 μf, 15 KV, 0.5 mm, Pressure

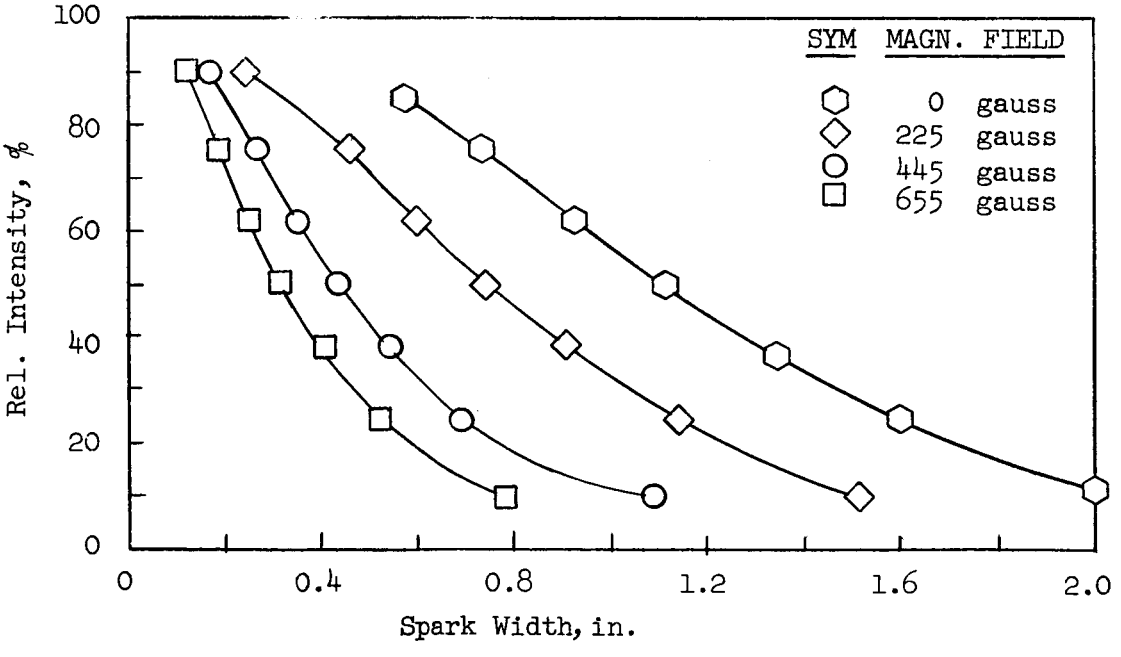

(b) 0.001 μf, 15 KV, 2 mm, Pressure

Fig. 2 SPARK INTENSITY PROFILES

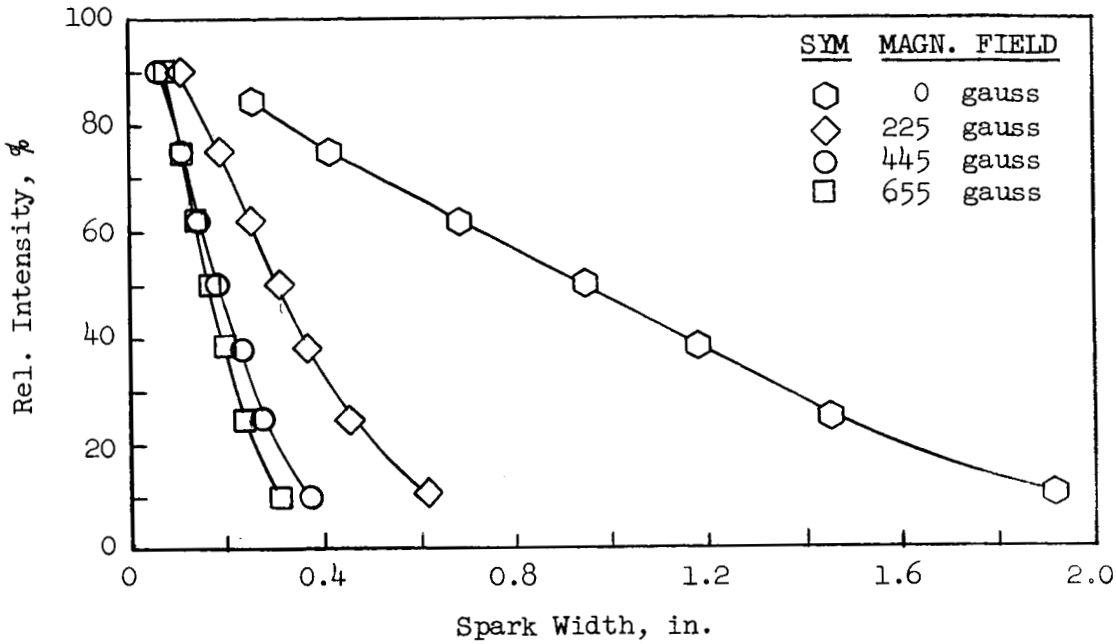

(c) 0.01 μf, 10 KV, 0.1 mm Pressure

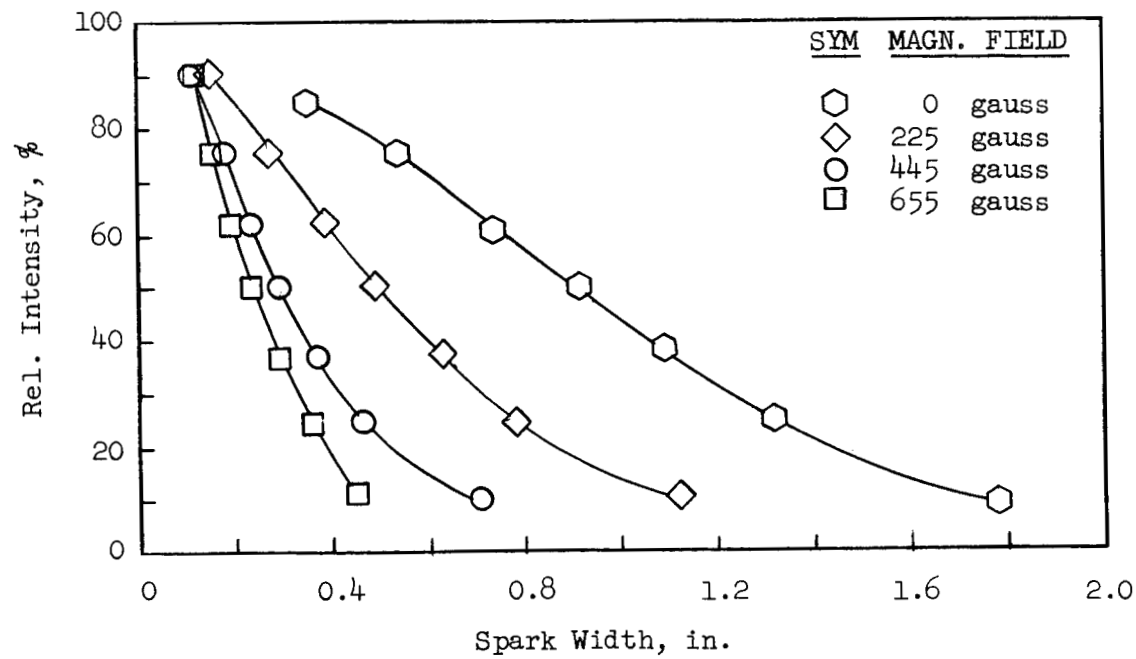

(d) 0.01 μf, 10 KV, 0.5 mm Pressure

Fig. 2 CONTINUED

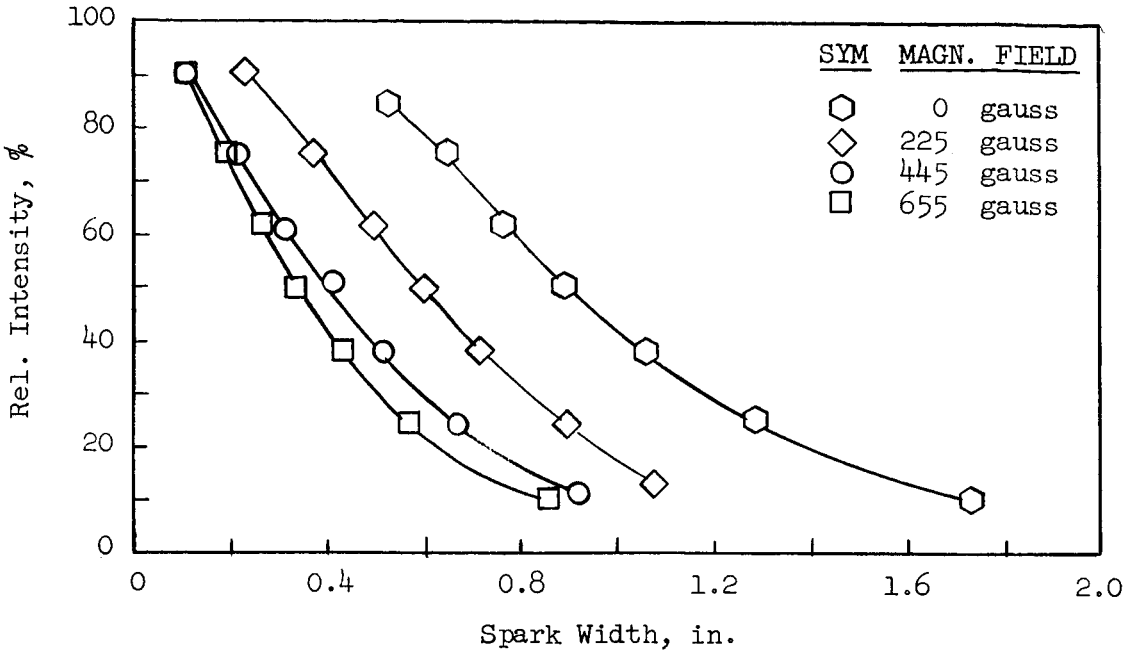

(e) 0.01 μf, 10 KV, 2 mm Pressure

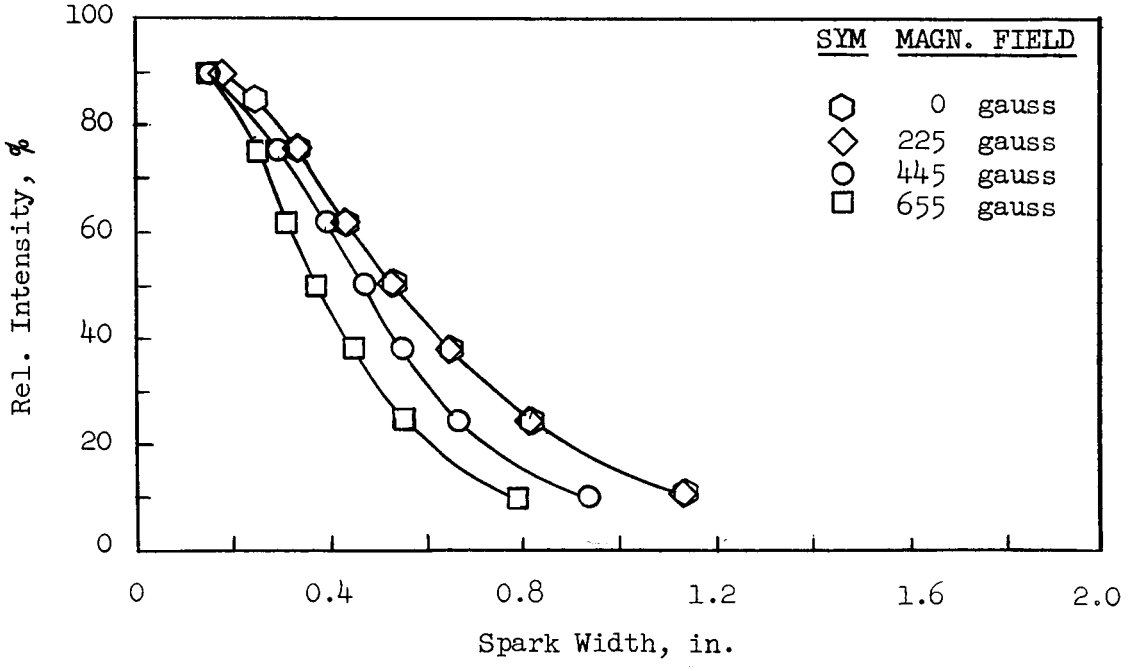

(f) 0.01 μf, 10 KV, 10 mm Pressure

Fig. 2 CONTINUED

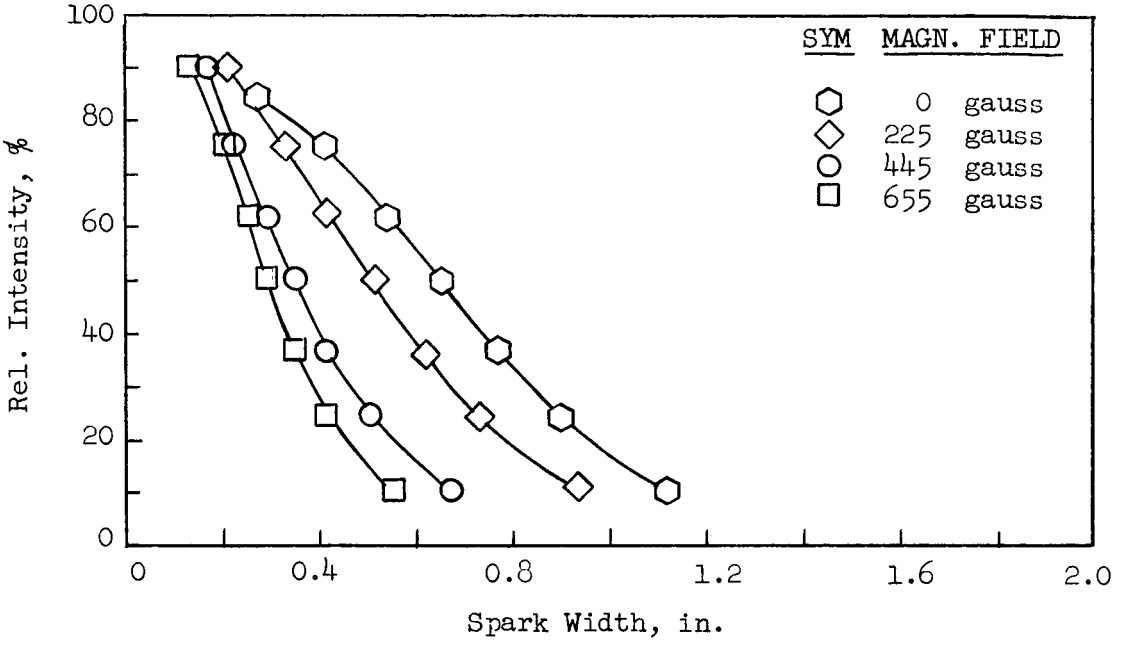

(g) 0.1 μf, 10 KV, 0.5 mm Pressure

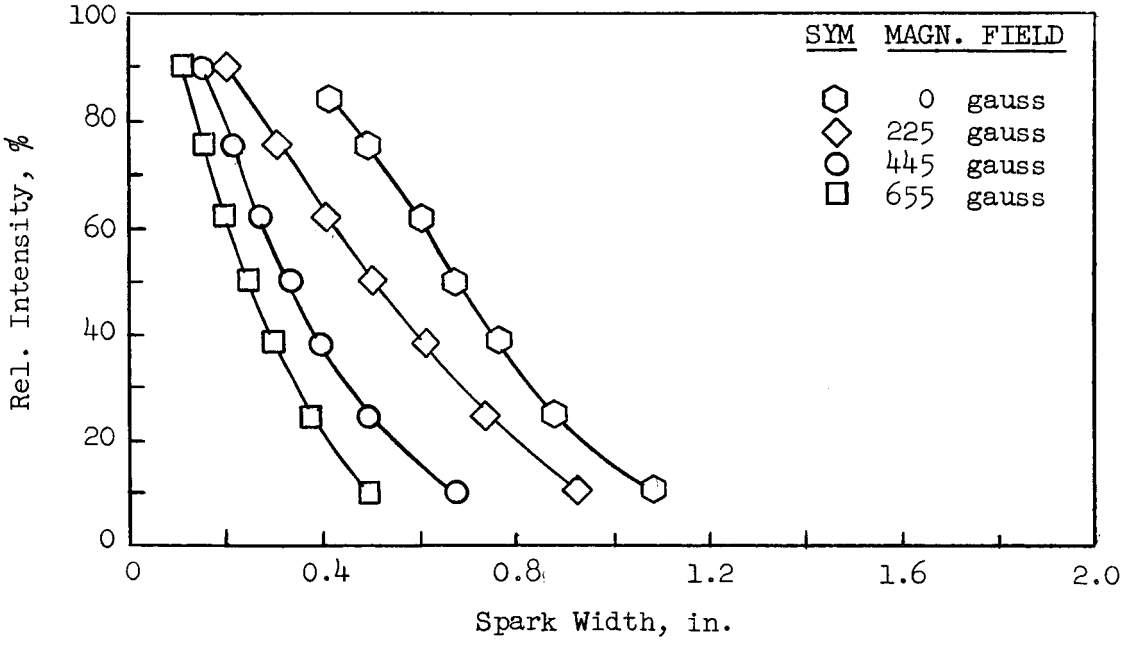

(h) 0.1 μf, 10 KV, 2 mm Pressure

Fig. 2 CONCLUDED

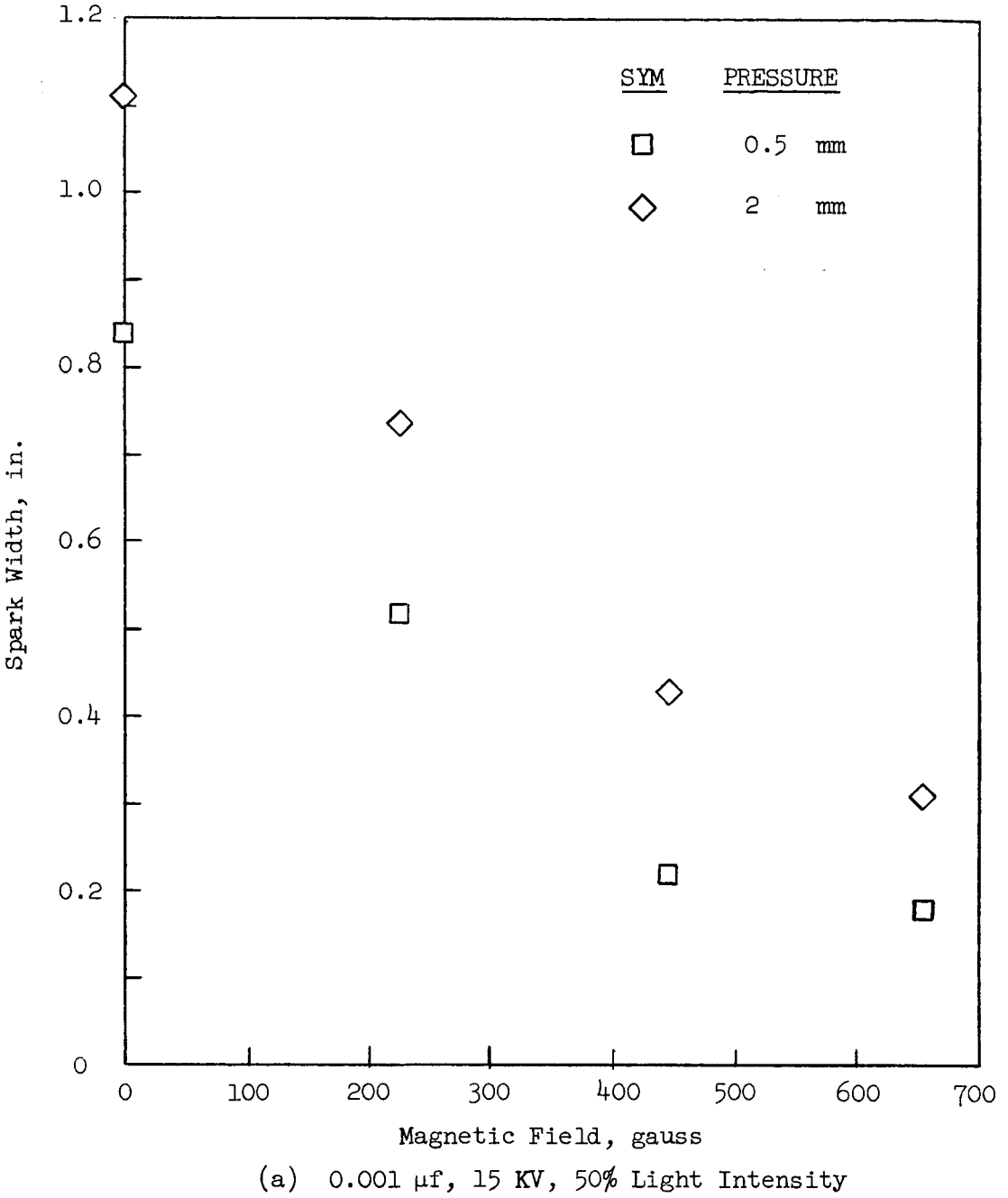

(a) 0.001 μf, 15 KV, 50% Light Intensity

FIG. 3 EFFECT OF MAGNETIC FIELD ON SPARK WIDTH

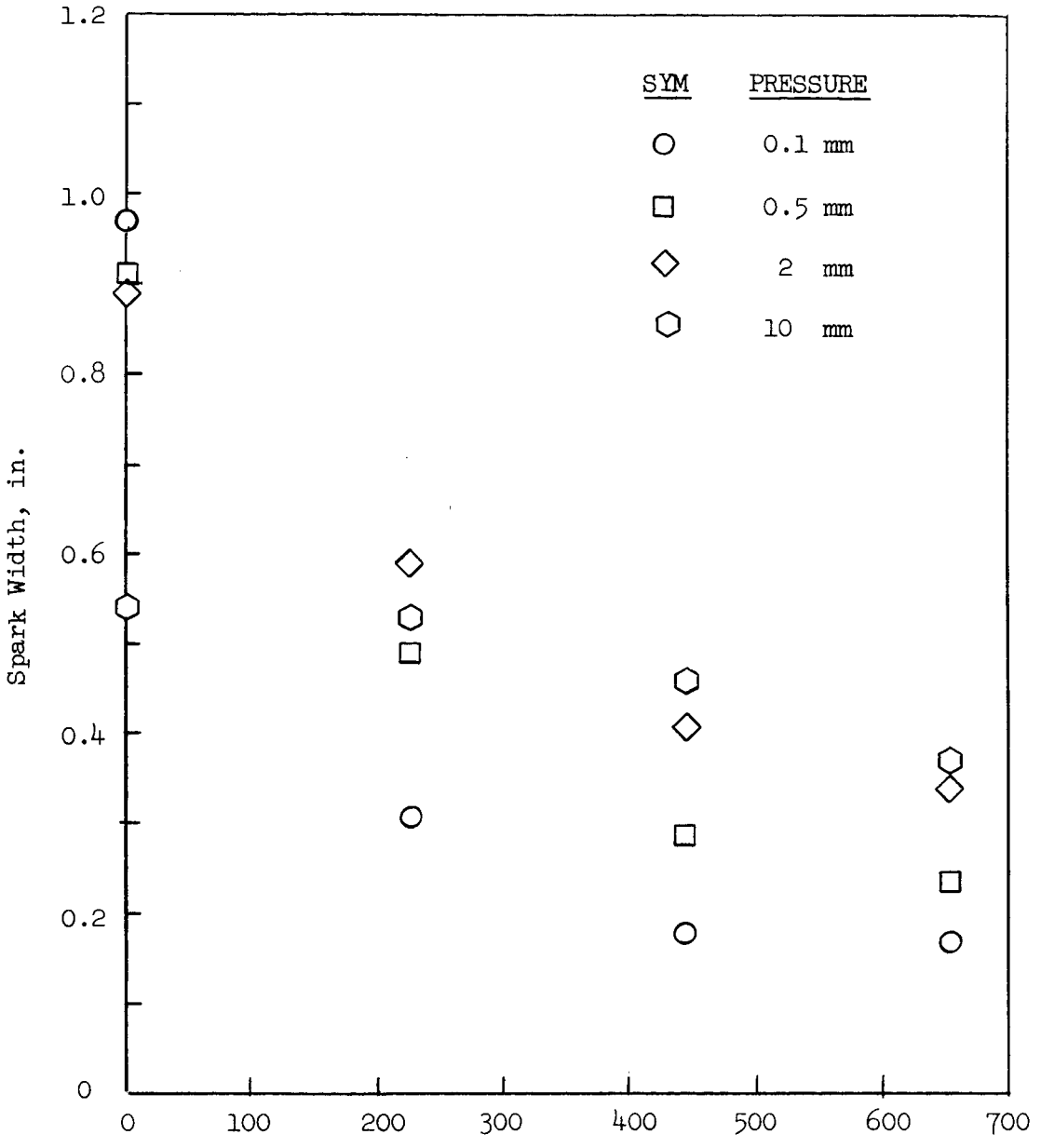

(b) 0.01 μf, 10 KV, 50% Light Intensity

FIG. 3 CONTINUED

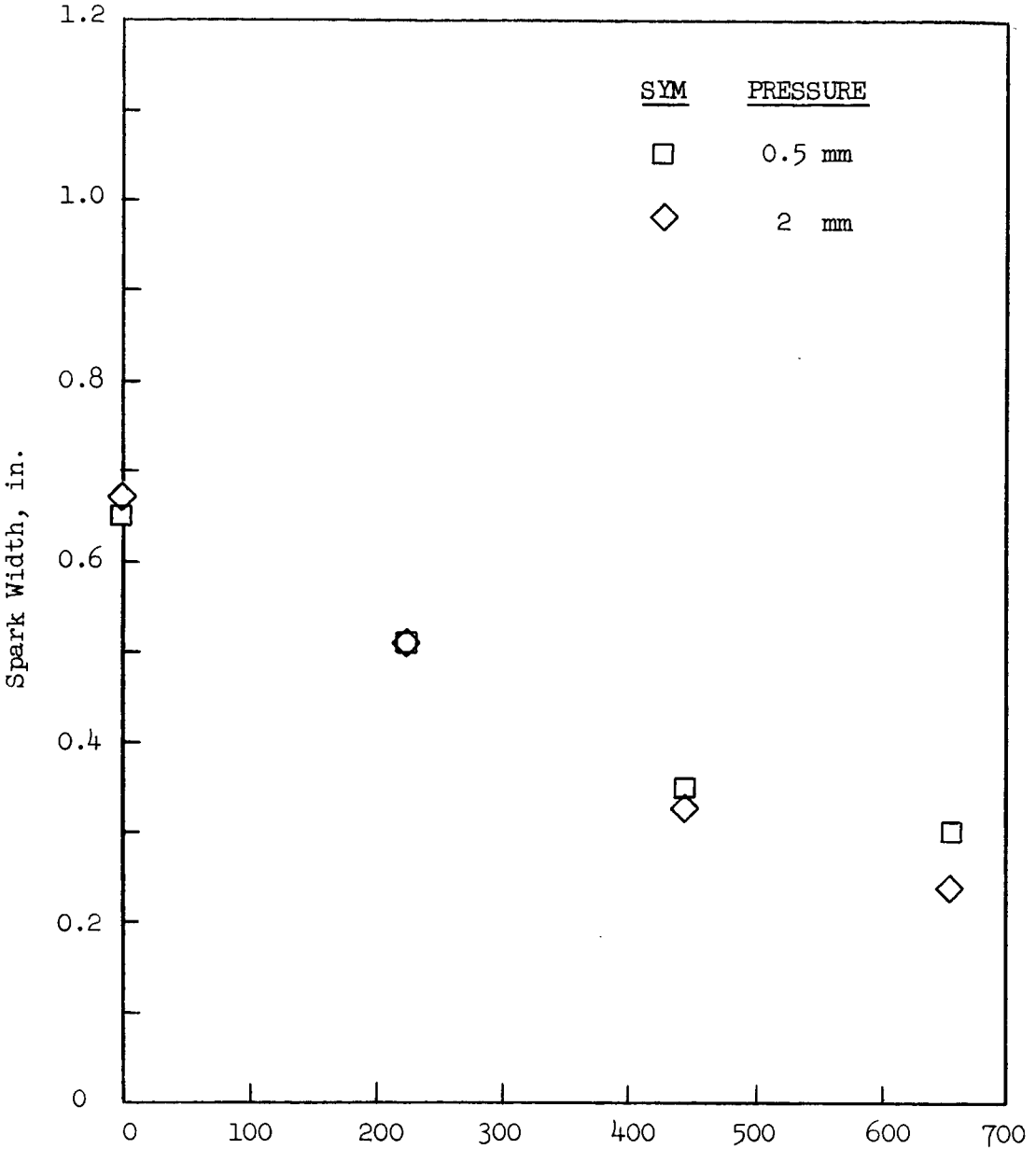

(c) 0.1 μf, 10 KV, 50% Light Intensity

FIG. 3 CONCLUDED

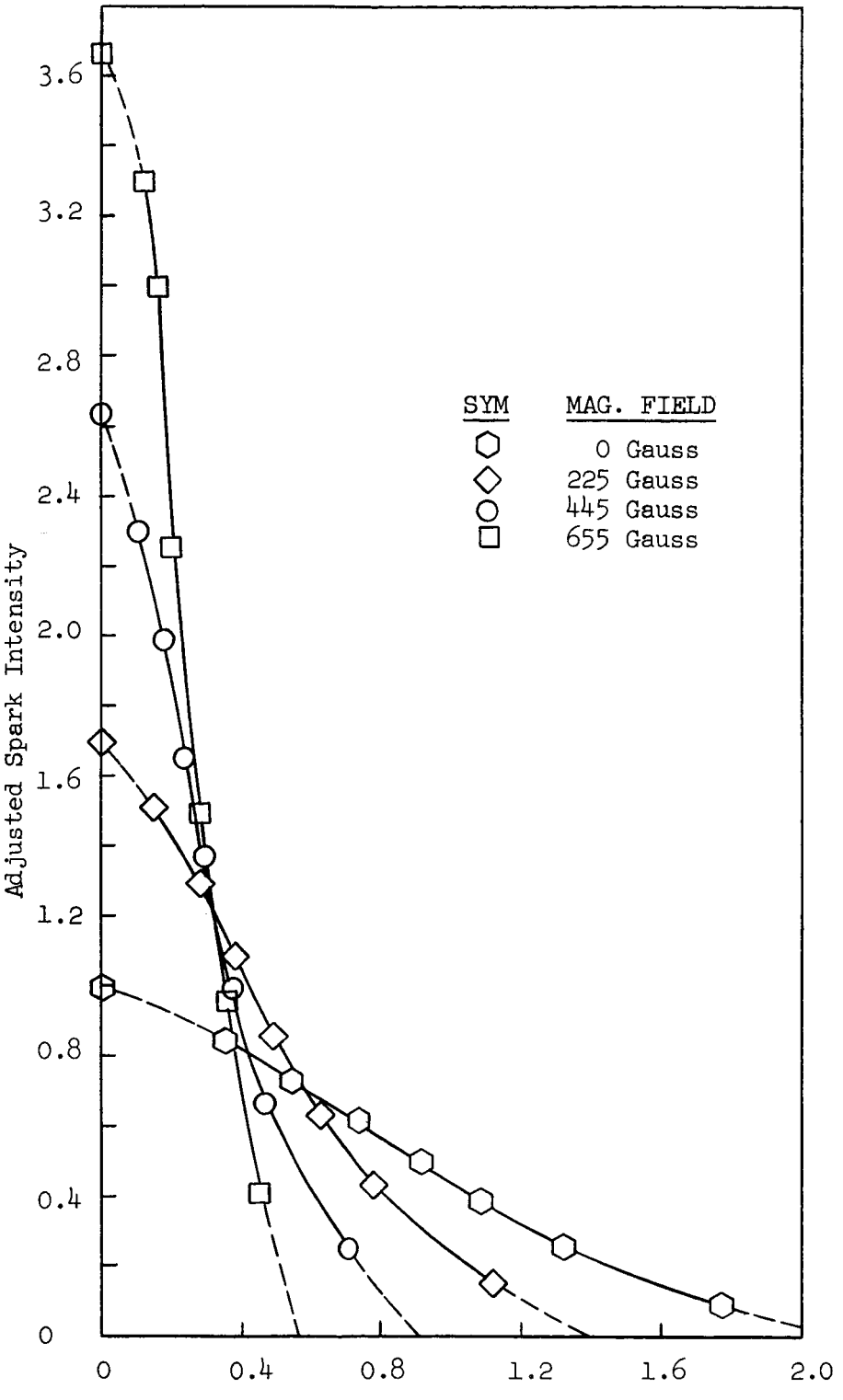

(a) 0.01μf, 10KV, 0.5mm Pressure

FIG. 4 ADJUSTED SPARK INTENSITY PROFILES

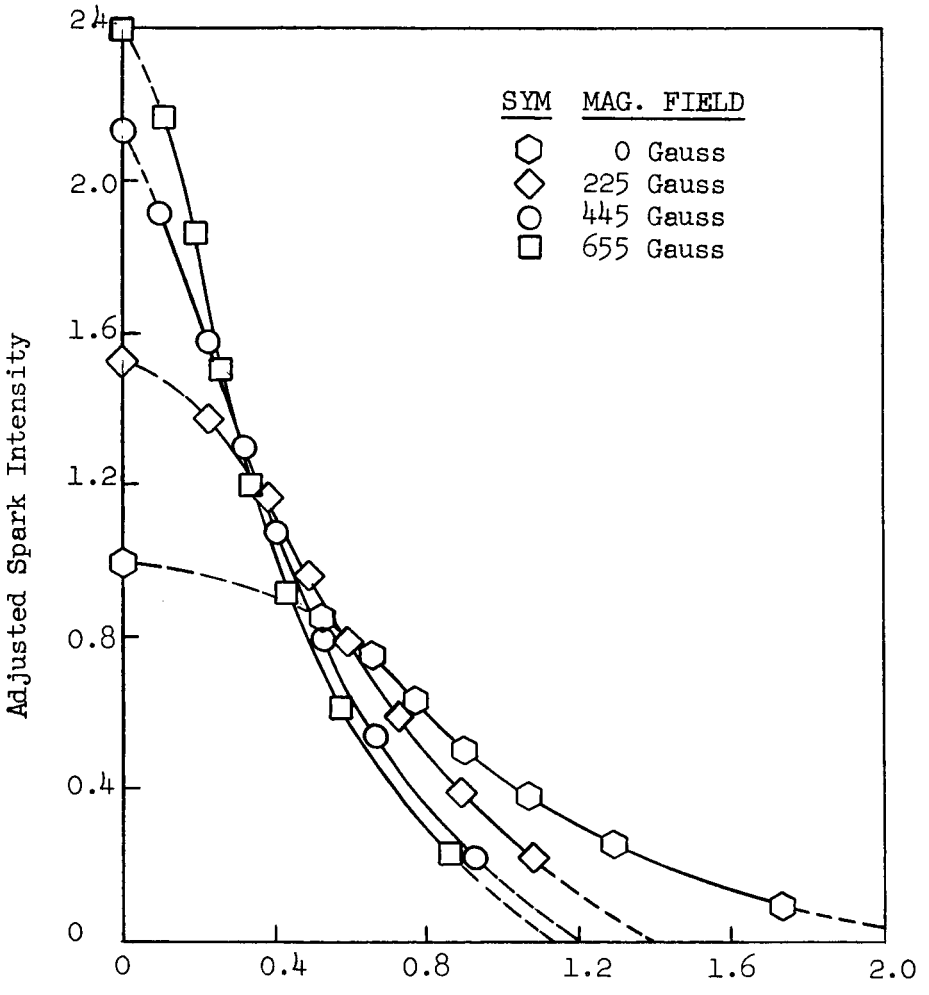

(b) 0.01μf, 10KV, 2mm Pressure

FIG. 4 Concluded

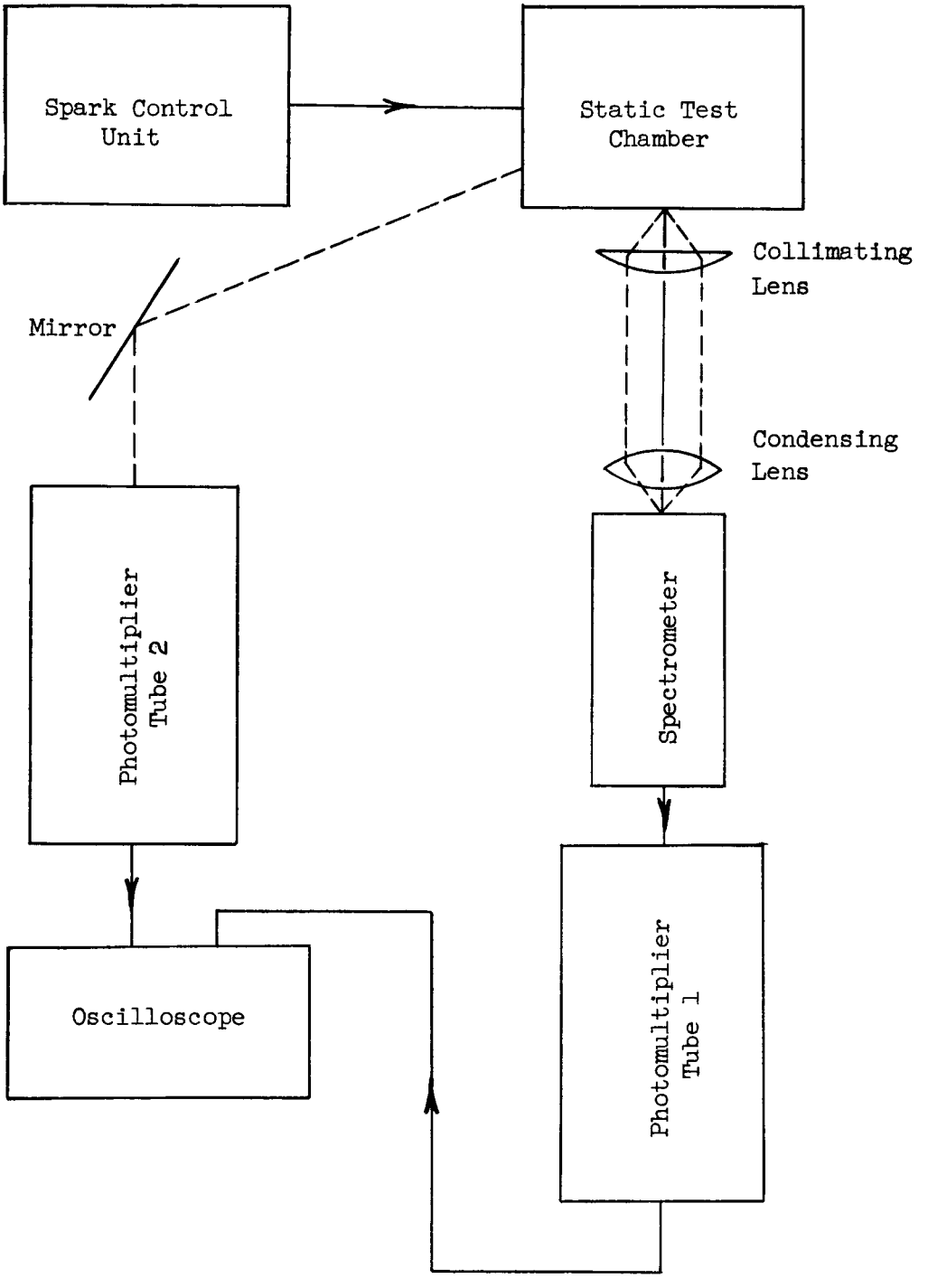

FIG. 5 SCHEMATIC DIAGRAM OF APPARATUS FOR SPARK-TEMPERATURE MEASUREMENT

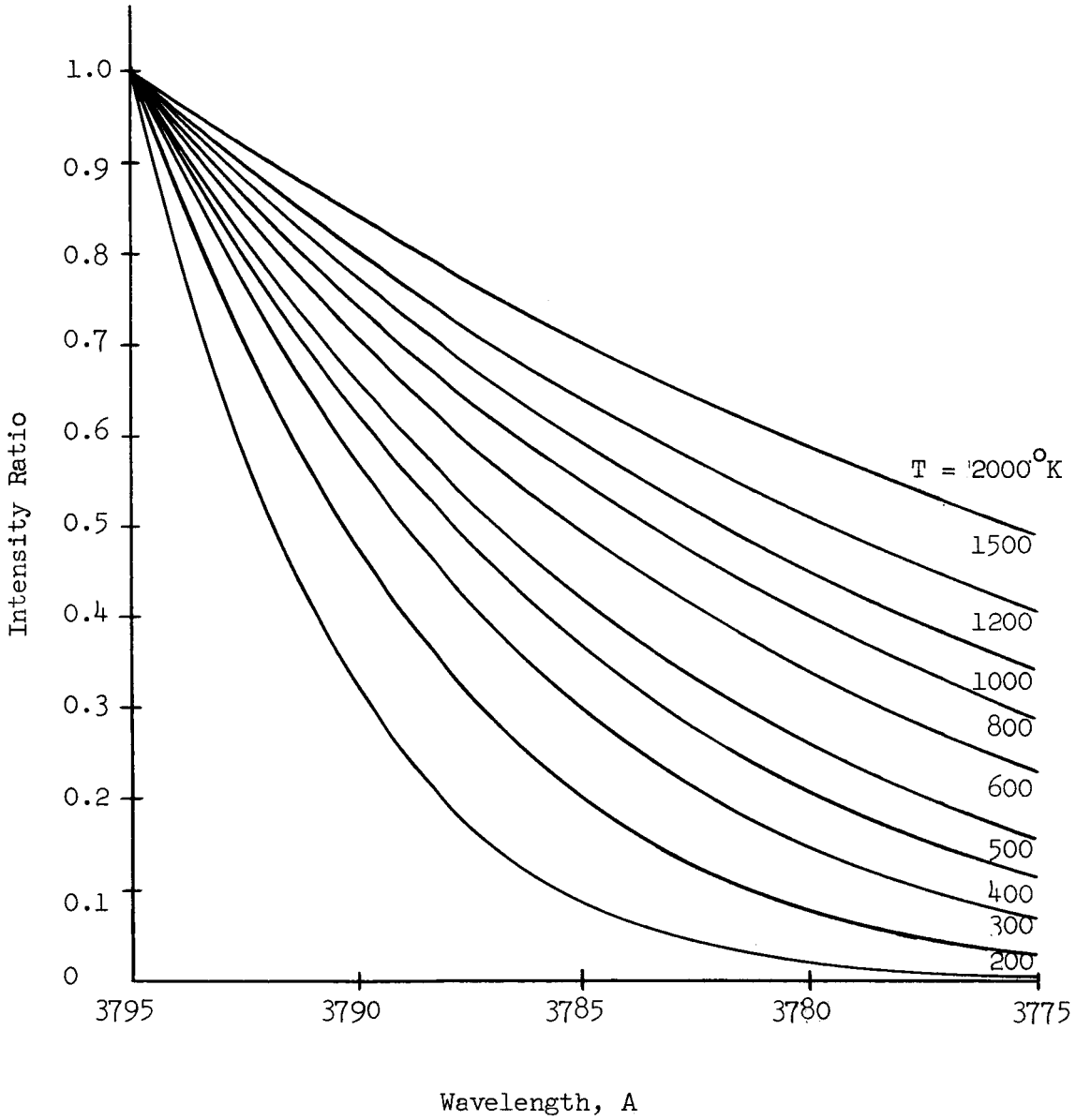

FIG. 6 EFFECT OF ROTATIONAL TEMPERATURE ON BAND STRUCTURE
0,2 BAND NITROGEN SECOND POSITIVE SYSTEM

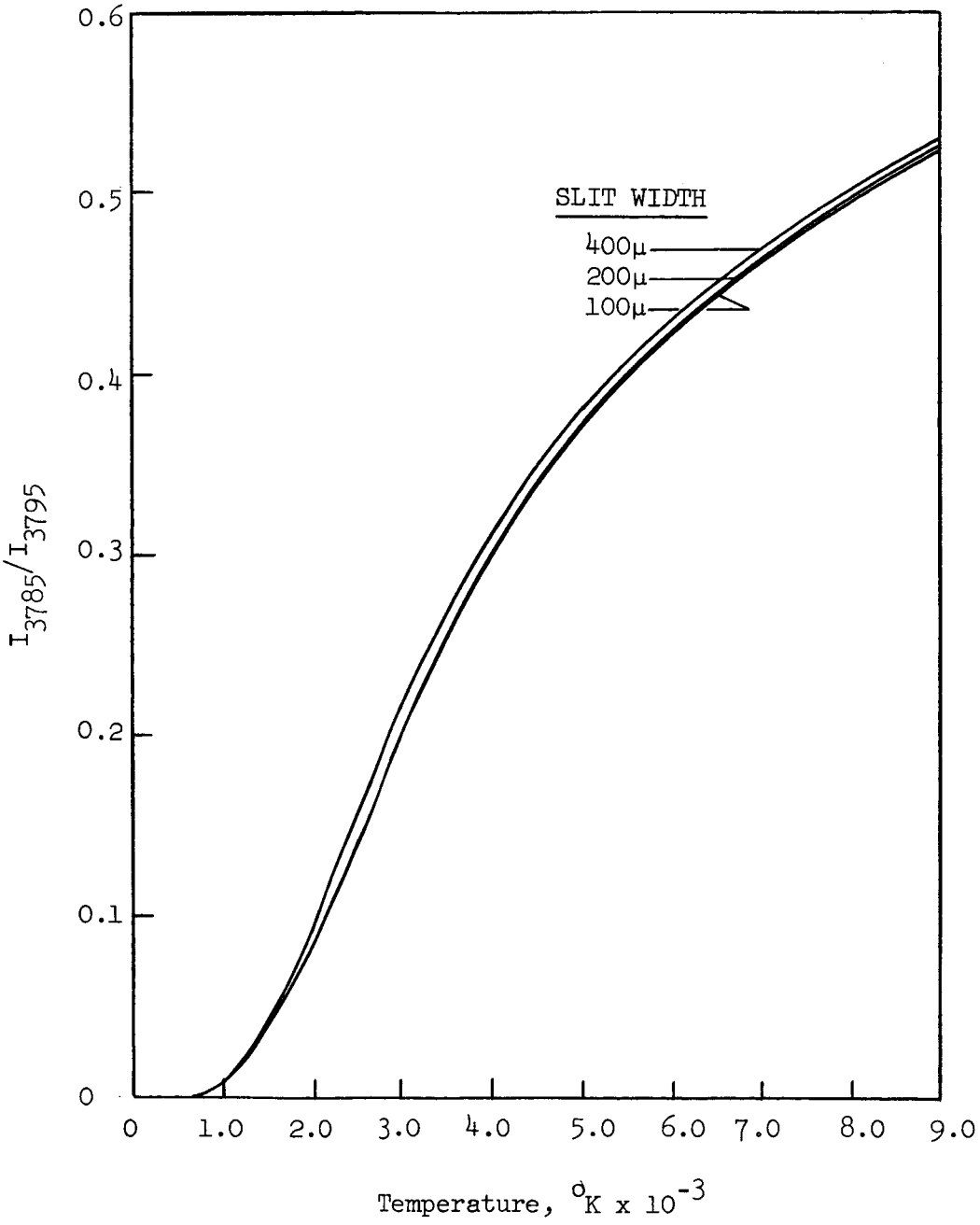

FIG. 7 INTENSITY RATIO VS. TEMPERATURE

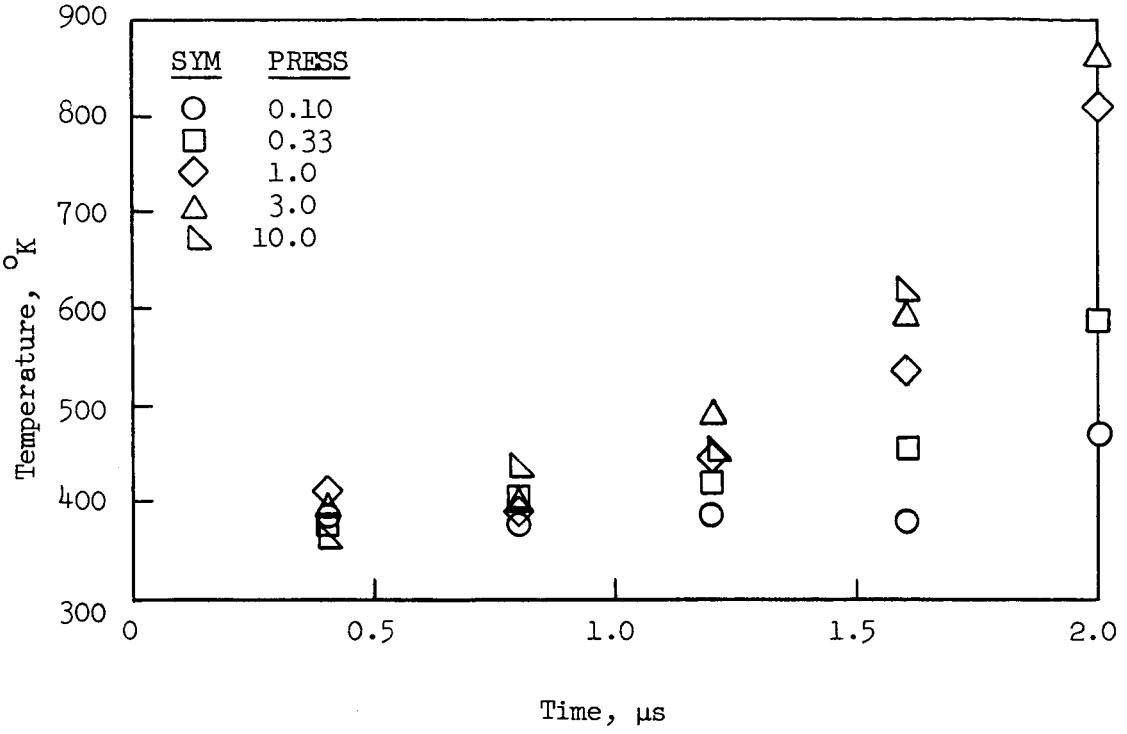

(a) 0 Gauss

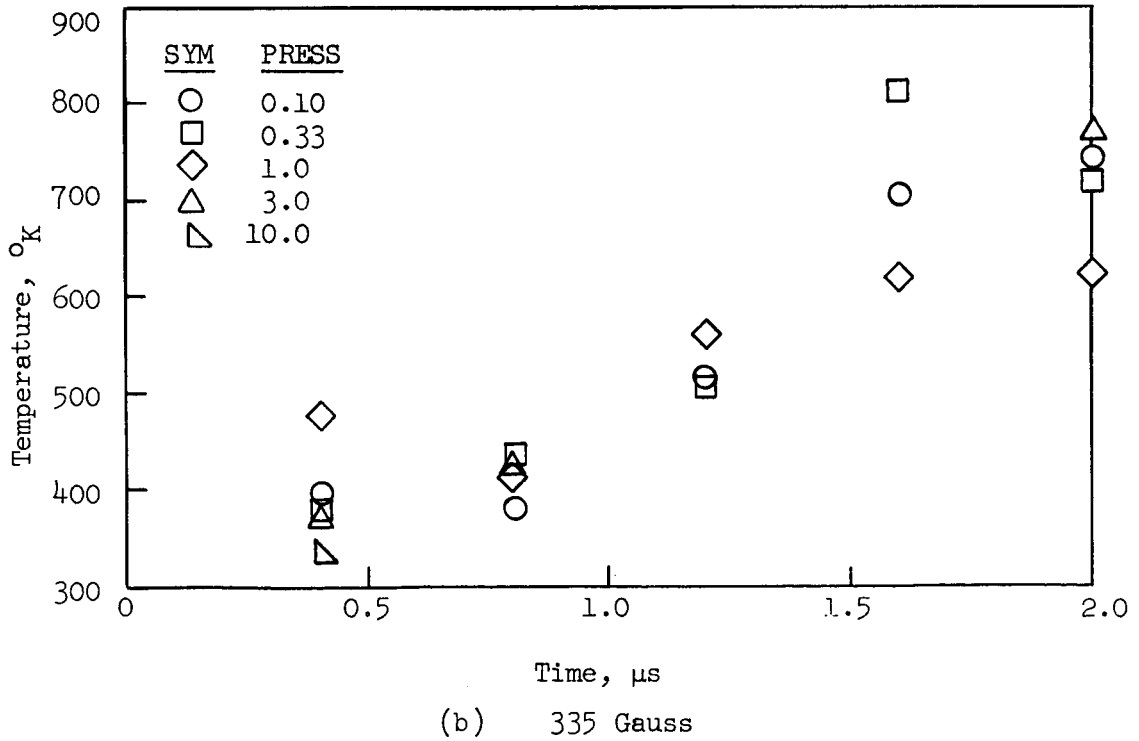

(b) 335 Gauss

FIG. 8 SPARK HEATING PLATES, 5-JOULE SPARK

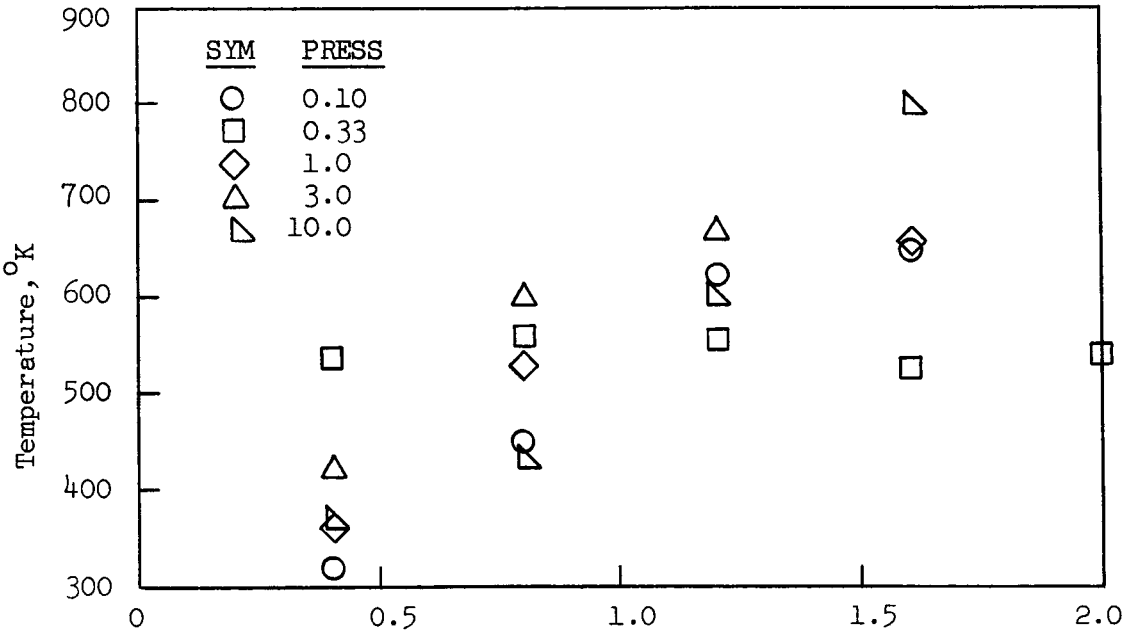

(c) 665 Gauss

FIG. 8 Concluded

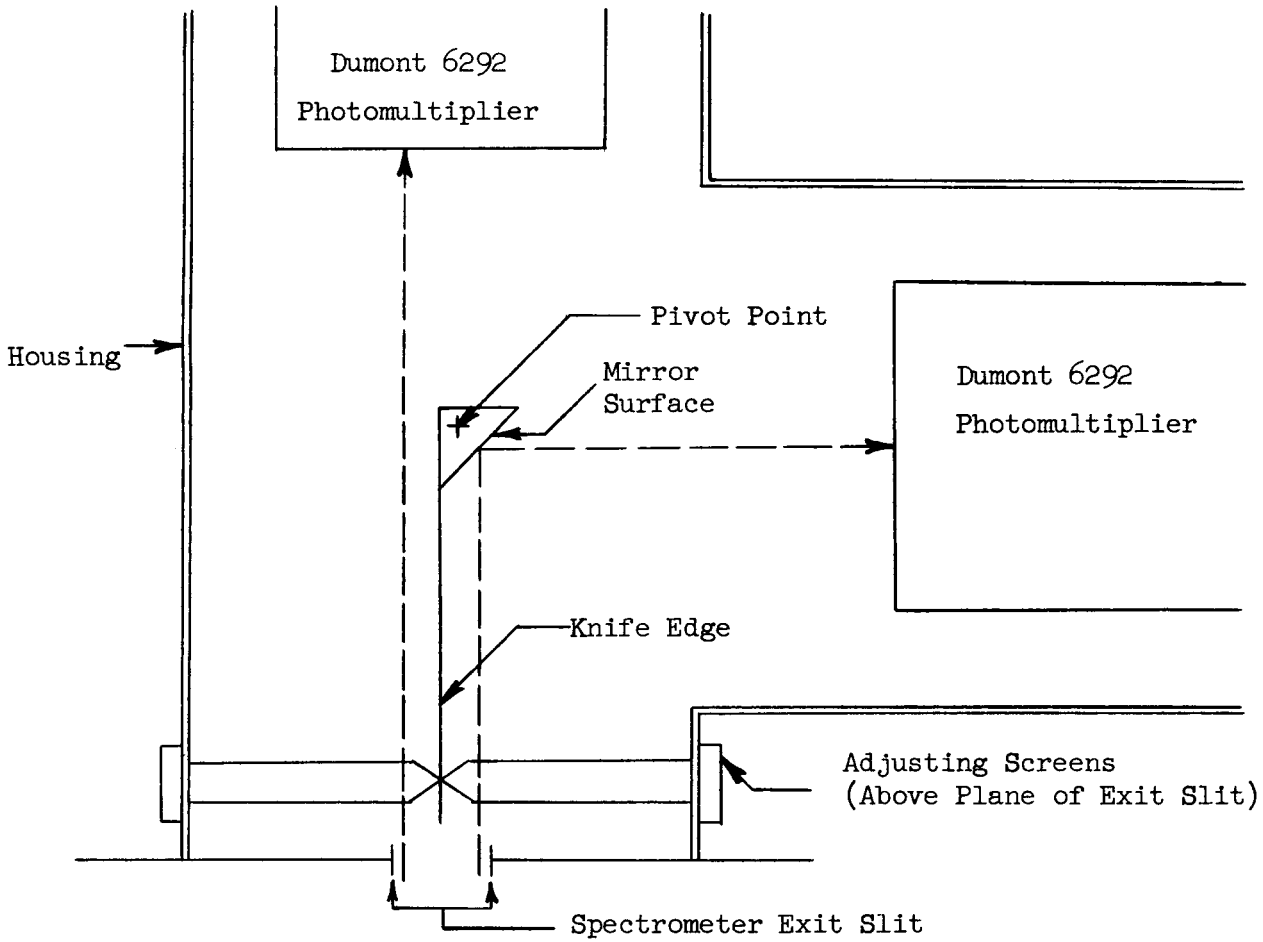

FIG. 9. DIAGRAM OF TWO-CHANNEL PHOTOMULTIPLIER HEAD